Low-Voltage, Flexible and Self-Encapsulated Ultracompact Organic Thin-Film Transistors Based on Nanomembranes

Kleyton Torikai,[†,‡] *Rafael Furlan de Oliveira,*[†] *Davi H. Starnini de Camargo,*[†,‡] *and Carlos C. Bof Bufon*[†,‡*]

† Brazilian Nanotechnology National Laboratory (LNNano), Brazilian Center for Research in Energy and Materials (CNPEM), 13083-970 Campinas, São Paulo, Brazil

‡ Postgraduate Program in Materials Science and Technology (POSMAT), São Paulo State University (UNESP), 17033-360 Bauru, São Paulo, Brazil

* Corresponding Author: cesar.bof@lnnano.cnpem.br

Supporting Information

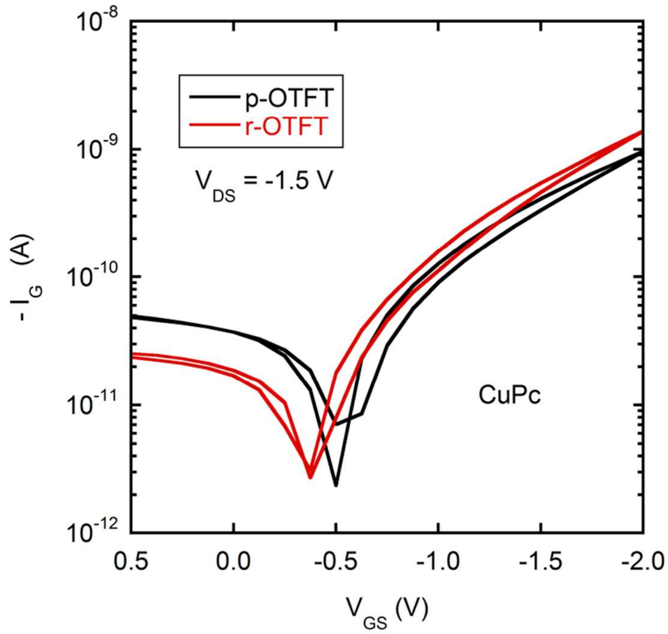

Figure S1. Gate leakage curves of CuPc OTFTs for both architectures.

Calculation of the dielectric specific capacitance (C_I)

The relative permittivity of the Al_2O_3 gate dielectric layer was obtained from the fabrication of several simple capacitors and measuring the capacitance at 1 kHz. The average value found is $\varepsilon_r = 5.6$. Assuming that the n-octadecylphosphonic acid self-assembled monolayer (ODPA-SAM) thickness is 2.1 nm and its relative permittivity[1] is 2.5, we calculate the specific capacitance:

$$C_{\mathrm{total}} = \left(\frac{1}{C_{\mathrm{SAM}}} + \frac{1}{C_{\mathrm{Al_2O_3}}}\right)^{-1} \cong \ 200\ \mathrm{nF{\cdot}cm^{-2}}$$

Unipolar inverters fabricated with r-OTFTs

One advantage of the use of standard microfabrication techniques for OTFT fabrication lies on the production of several devices on the same chip. Thus, a simple circuit application involving the connection of nearby OTFTs is the operation of unipolar inverters.[2] Here, we employed wire bonding technology for this purpose, although interconnects can be readily designed and assembled during the OTFT fabrication. Figure S2 shows the electrical characteristics of a unipolar p-type inverter formed by the association of two CuPc r-OTFTs.

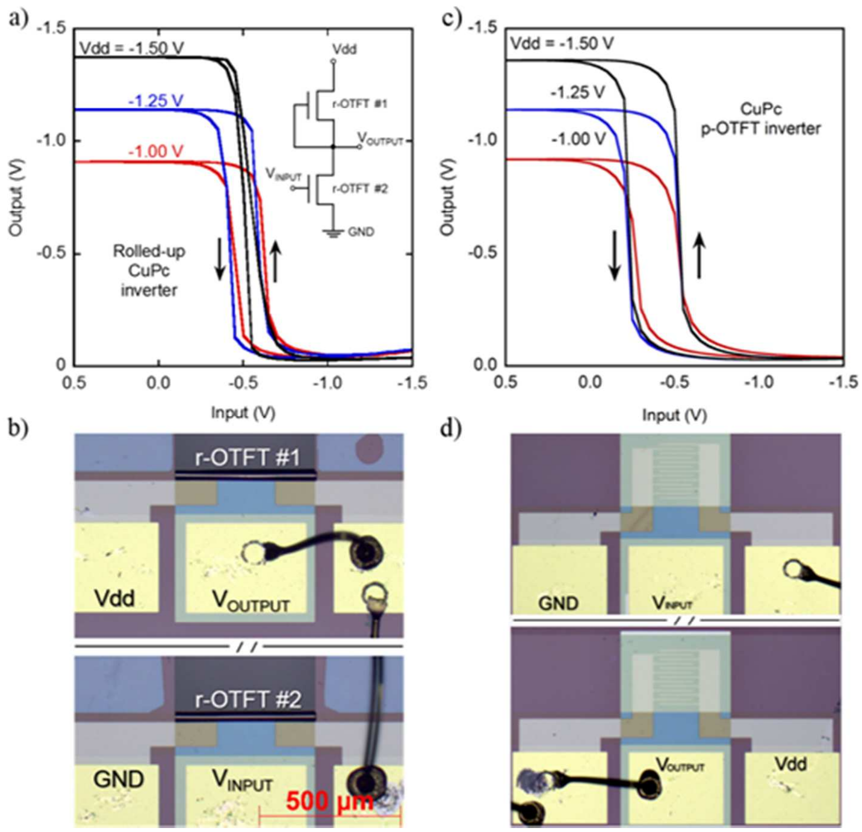

Figure S2. Unipolar p-type inverter based on CuPc OTFTs. (a) The electrical response of r-OTFT unipolar inverter. Inset: respective unipolar inverter circuit. (b) Optical microscopy image is showing the association of two CuPc r-OTFTs through wire bonding for the inverter operation. (c) Electrical response of p-OTFT inverter and its (d) respective microscopy image. The measurements were carried out at room temperature in a laboratory atmosphere.

From the inverter characteristics (Figure S2a), we observe an output signal compromised in *ca.* 8% for supply voltages (V_{dd}) of -1.0, -1.5, and -2.0 V. This may be a result of the gate leakage current experienced by the individual r-OTFTs or contact issues. Moreover, although a reasonable sharp switching is observed, considerable hysteresis in the inverter response is present. The observed hysteresis is also related to the inherent hysteresis shown by the individual r-OTFTs in the main text (Figure 2f). The association of two hysteretic r-OTFTs worsens the inverter performance. For better inverter responses though, the electrical characteristics of the individual r-OTFTs have to be improved. Nevertheless, we emphasize the measured inverter characteristics are not inferior to those involving p-OTFTs (Figure S2c), which again corroborates the feasibility of our strategy for the fabrication of ultracompact organic devices.

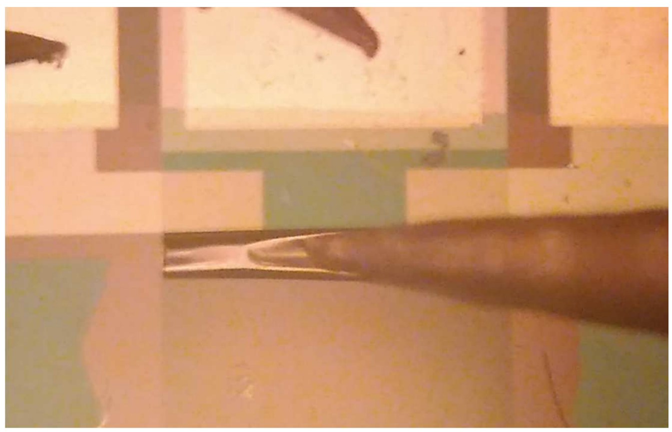

Figure S3. Static compression of the CuPc r-OTFT by a rounded needle tip.

Table S1. CuPc r-OTFT electrical characteristics throughout mechanical stress.

	μ (10^{-3} cm^2/Vs)	**V_{TH} (V)**	**ON/OFF ratio (A/A)**	**g_m (nS)**
Before compression	1.5	0.04	$\propto 10^3$	86
Under compression	1.6	0.00	$\propto 10^3$	86
Compression released	1.6	-0.04	$\propto 10^3$	89

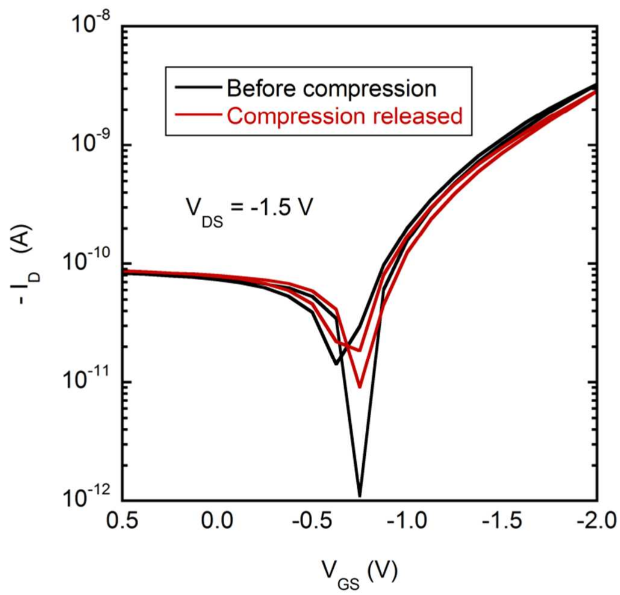

Figure S4. Gate leakage current during static mechanical compression.

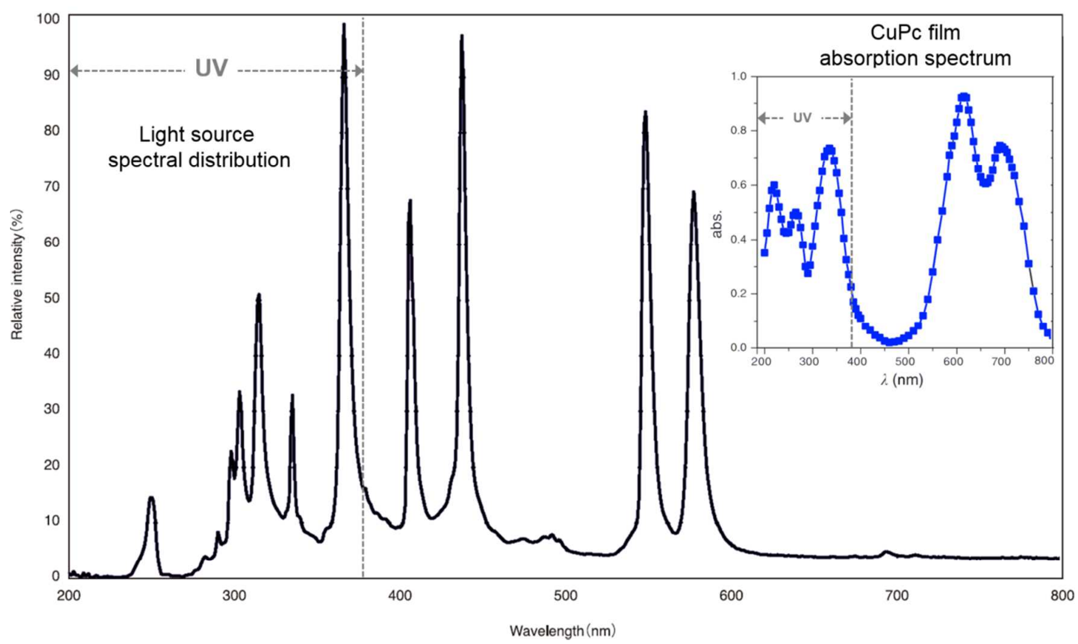

Figure S5. Mercury lamp emission spectrum. Inset: absorption spectrum of CuPc thin-films adapted from Farag et al.[3]

Estimated UV transmittance through r-OTFTs

To provide an upper limit to the transmittance of UV radiation through the nanomembrane (NM), we consider only the metallic strained bilayer (Ti/Cr in 15 nm/20 nm). Estimating the transmittance (T) considering internal transmission only, which follows Lambert's law:

$$T = e^{-\int_0^l \alpha(z)\,dz}$$

with l being the total thickness and $\alpha(z)$ the attenuation coefficient at depth z into the material. From the complex refractive index tables,[4] the attenuation coefficient is obtained by:

$$\alpha = \frac{4\pi\kappa}{\lambda_0}$$

with λ_0 being the vacuum wavelength. For $\lambda_0 = 365$ nm, the calculated transmittance through the NM bilayer is ~3.5%.

Table S2. DNTT OTFTs electrical characteristics for both p- and r- architectures.

DNTT OTFT	μ (10^{-3} cm^2/Vs)	V_{TH} (V)	ON/OFF ratio (A/A)	g_m (nS)
p-	6.7	0.38	$\propto 10^3$	55
r-	13.5	-0.64	$\propto 10^3$	67

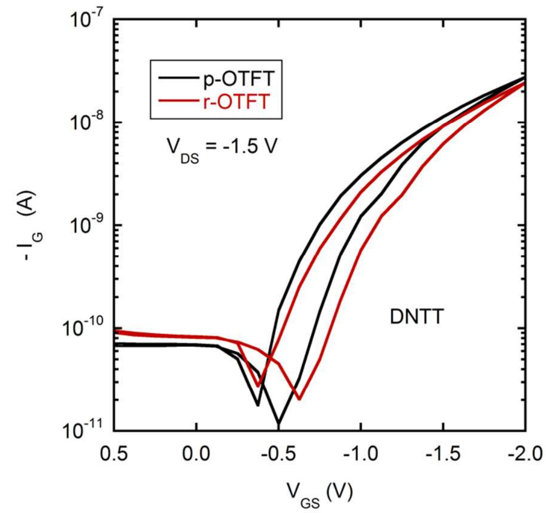

Figure S6. Gate leakage curves of DNTT OTFTs for both architectures.

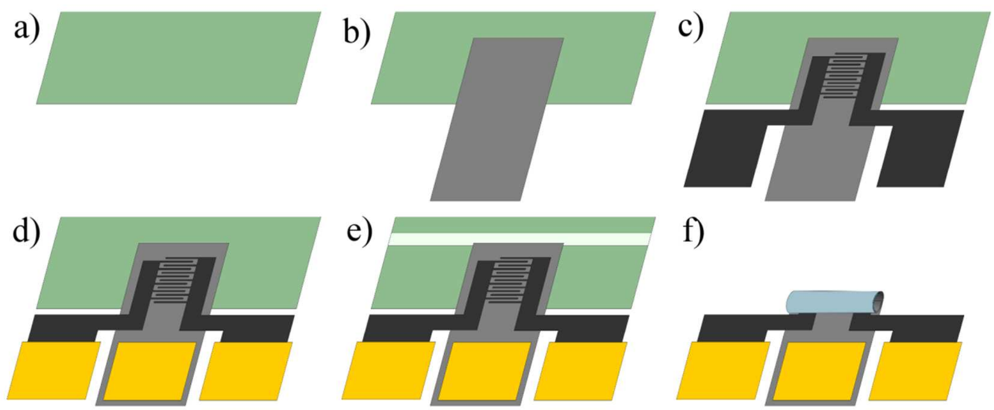

Figure S7. Main step-by-step fabrication schematics. (a) GeOx sacrificial layer followed by SiO_2 and Al_2O_3 external insulator. (b) Ti/Cr strained bi-layer and the Al_2O_3 gate dielectric. (c) Cr/Au source and drain interdigitate electrodes. (d) Cr/Au contact pads. (e) Etching of oxide layers to allow H_2O_2 aqueous solution access to the sacrificial layer from the top of the device. (f) After the OSC deposition, removal of the sacrificial layer causes the device to roll-up in an ultra-compact tubular shape.

REFERENCES

(1) Klauk, H.; Zschieschang, U.; Pflaum, J.; Halik, M. *Nature* 2007, *445* (7129), 745–748.
(2) Brown, A. R.; Jarrett, C. P.; de Leeuw, D. M.; Matters, M. *Synth. Met.* 1997, *88* (1), 37–55.
(3) Farag, A. A. M. *Opt. Laser Technol.* 2007, *39* (4), 728–732.
(4) Johnson, P.; Christy, R. *Phys. Rev. B* 1974, *9* (12), 5056–5070.